Journal of Materials Chemistry A

Anomalous enhancement of thermoelectric power factor by thermal management with resonant level effect

Journal:	*Journal of Materials Chemistry A*
Manuscript ID	TA-ART-09-2020-008683.R1
Article Type:	Paper
Date Submitted by the Author:	26-Dec-2020
Complete List of Authors:	Sakane, Shunya; Osaka University Graduate School of Engineering Science School of Engineering Science, Ishibe, Takafumi; Osaka University Mizuta, Kosei; Osaka University Graduate School of Engineering Science School of Engineering Science Fujita, Takeshi; KUT, School of Environmental Science and Engineering; Kochi University of Technology Kiyofuji, Yuga; Toho University Faculty of Science Graduate School of Science Ohe, Jun-ichiro; Toho University Faculty of Science Graduate School of Science Kobayashi, Eiichi; Kyushu Synchrotron Light Research Center, Nakamura, Yoshiaki; Osaka Univ, Grad Sch Engn Sci

SCHOLARONE™
Manuscripts

ARTICLE

Anomalous enhancement of thermoelectric power factor by thermal management with resonant level effect

Received 00th January 20xx,
Accepted 00th January 20xx

DOI: 10.1039/x0xx00000x

Shunya Sakane[a], Takafumi Ishibe[a], Kosei Mizuta[a], Takeshi Fujita[b], Yuga Kiyofuji[c], Jun-ichiro Ohe[c], Eiichi Kobayashi[d], and Yoshiaki Nakamura*[a]

Obtaining high thermoelectric performance has been the biggest historical challenge for thermoelectric generation. Here, we propose a methodology of thermoelectric power factor enhancement: thermal management with resonant level effect for simultaneous increase of electrical conductivity σ and Seebeck coefficient S. Au crystals and Au impurities are introduced into SiGe. Therein, (1) highly-conductive Au crystals increased σ. (2) Au impurities brought resonant level effect and phonons scattering, resulting in enhanced S and lowered thermal conductivity κ of SiGe. (3) This κ distribution control brings focus of temperature difference on SiGe parts with lowered κ, resulting in the availability of the enhanced S of SiGe parts as effective S of the entire nanocomposites. Consequently, we achieved the highest $S^2\sigma$ at room temperature among SiGe-related materials ever reported. Electronic structure calculation and measurement support the existence of resonant level, which enhances S and lowers κ. These results provide a new route to the thermoelectric performance enhancement.

Introduction

Thermoelectric conversion is attracted as one of the energy harvesting techniques. Its efficiency increases as dimensionless figure of merit ZT (=$S^2\sigma T/\kappa$) increases, where S is Seebeck coefficient, σ is electrical conductivity, κ is thermal conductivity, and T is absolute temperature. For ZT increase, power factor ($S^2\sigma$) enhancement and κ reduction are required. However, it is challenging to control three properties (S, σ, and κ) independently due to their trade-off relationships. In many reports that have ever been published, phonon scattering at nanostructure interfaces brought κ reduction, resulting in ZT enhancement[1-16]. Recently, for further ZT increase, $S^2\sigma$ enhancement by controlling electronic states and carrier scattering has been drawing much attention[17-27].

Resonant level effect (RLE) approach is one of the most effective $S^2\sigma$ enhancement methods. There have been many reports about $S^2\sigma$ enhancement by RLE in various thermoelectric materials with impurities[28-36]. Therein, the resonant energy level position related to impurities is in the conduction (valence) band and very close to the conduction (valence) band edge in n- (p-) type semiconductor[37], and conducting carriers are influenced by the resonant level, leading to S increase. However, in general, due to the concomitant σ degradation, RLE is not always beneficial for thermoelectric properties[37]. $S^2\sigma$ is enhanced only when S increase effect is larger than σ decrease effect[37]. Thus, in RLE, the accompanying σ degradation limits $S^2\sigma$ enhancement.

On the other hand, in our previous report, we proposed the methodology of $S^2\sigma$ enhancement in p-type SiGe-Au composites that are composed of SiGe and Au parts by thermal management[38]. Therein, Au crystal parts, leading to high σ, have high κ and Ge-rich SiGe nanograins have low κ due to phonon transport control by the nanograin structures. Therefore, large temperature difference (ΔT) is mainly applied to nanostructured Ge-rich SiGe parts that have high S (thermal management). As a result, the high S of Ge-rich SiGe parts is available as effective S of entire composite. Thus, this thermal management leads to increase of σ due to Au parts while keeping high S of SiGe parts. The detail of the temperature difference of composite materials is shown in Fig. S1 ESI.†. Such thermal management can be a way to compensate the weakness (σ degradation) of RLE approach. The combination of two approaches can realize simultaneous increase of S and σ toward further $S^2\sigma$ enhancement. However, it is a big challenge to control the two kinds of quanta: electron and phonon, simultaneously.

[a] Graduate School of Engineering Science, Osaka University, 1-3 Machikaneyama-cho, Toyonaka, Osaka 560-8531, Japan.
[b] School of Environmental Science and Engineering, Kochi University of Technology, 185 Miyanokuchi, Tosayamada, Kami, Kochi 782-8502, Japan.
[c] Department of Physics, Toho University, 2-2-1 Miyama, Funabashi, Chiba, 274-8510, Japan.
[d] Kyusyu Synchrotron Light Research Center, 8-7, Yayoigaoka, Tosu-shi, Saga, 841-0005, Japan.
† Footnotes relating to the title and/or authors should appear here.
Electronic Supplementary Information (ESI) available: [details of any supplementary information available should be included here]. See DOI: 10.1039/x0xx00000x

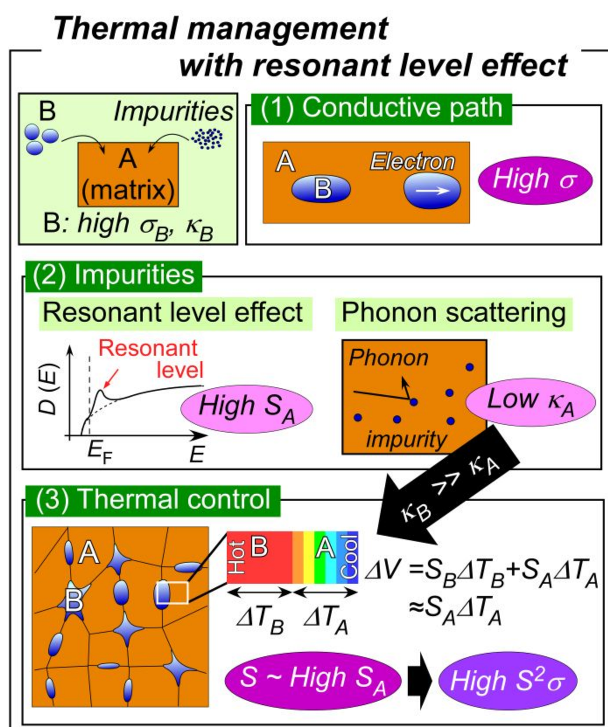

Fig. 1 The conceptual diagram of our proposed methodology for the enhancement of thermoelectric performance: thermal management with RLE. Therein, (1) material B with high electrical conductivity (σ_B) working as conductive path increases σ of the entire material. (2) Impurities bring RLE and phonons scattering, resulting in enhancing S and lowering κ of material A (S_A and κ_A). (3) This enhanced high S_A is available as the effective S of the entire material because ΔT is applied to material A with lowered κ_A, not to material B with low S_B. ΔV is thermoelectromotive force.

We propose a methodology of further $S^2\sigma$ enhancement by electron interaction and phonon scattering through resonant level impurity: thermal management with RLE, as shown in Fig. 1. In the thermal management with RLE approach, impurity introduction into material A enhances S_A by RLE and reduces κ_A by phonon scattering at the resonant level impurity. Material B with high σ_B (low S_B and high κ_B) is introduced into such material A to increase σ of entire material. Although high σ material introduction reduces S of entire material because of its low S in general, the effective S of entire material is kept to be high RLE-enhanced S_A in the case of thermally-controlled material. Therein, the ΔT is mainly applied to material A with high S_A, not to material B with low S_B because κ_A is drastically reduced by phonon-scattering at resonant level impurity (thermal control). Here, we focus on SiGe crystal as material A, Au atom as a resonant level impurity in SiGe, and Au crystals as material B in Fig. 1 because of the abundant information about SiGe-related materials and industrial applicability. There have also been reports that Au-doped Si or Ge has resonant energy levels near the conduction band edge[39,40], which can increase S by RLE. We fabricate n-type Au-doped SiGe (called as SiGeAu sample in this paper) by suction casting method for $S^2\sigma$ enhancement by the thermal management with RLE. $S^2\sigma$ of the present nanocomposites exceed the maximum value of

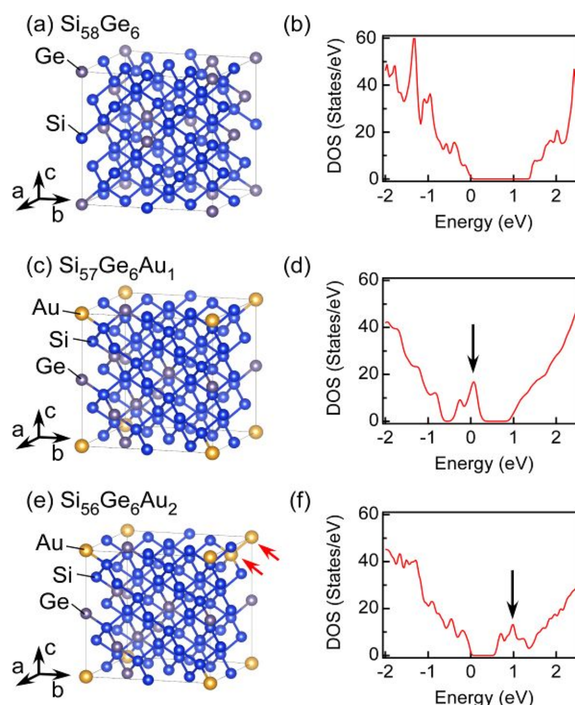

Fig. 2 Crystal structures of $Si_{58}Ge_6$ (a), $Si_{57}Ge_6Au_1$ (c), and $Si_{56}Ge_6Au_2$ (e). Calculated DOS of $Si_{58}Ge_6$ (b), $Si_{57}Ge_6Au_1$ (d), and $Si_{56}Ge_6Au_2$ (f). In (e), the arrows represent two Au atoms. In (d), the arrow represents (acceptor) energy levels in bandgap near valence band maximum formed by isolated Au impurities. In (f), the arrow represents resonant levels in conduction band near CBM formed by substitutional Au atoms.

SiGe-related materials that have ever been reported at room temperature (RT). This demonstrates that the thermal management with RLE related to the simultaneous control of electronic states and heat flow can bring giant thermoelectric power factor enhancement.

Results and discussion

The calculation of electronic states formed by substitutional Au atoms in SiGe.

Unlike reports about the density of states (DOS) calculation of Au-doped Si or Au-doped Ge[40], there has been few reports about DOS of Au-doped SiGe even though there has been a long history about SiGe study. Therefore, to confirm a resonant level in Au-doped "SiGe", we calculated electronic structures of Au-doped SiGe based on density functional theory (DFT) first-principle calculation by using Wien2k software package[41]. In this calculation, we use the k-points grid sampling of 5×5×5 for $Si_{56}Ge_6$, 14×14×14 for $Si_{57}Ge_6Au_1$ and $Si_{56}Ge_6Au_2$. It was confirmed that this calculation hardly depended on Ge distribution in SiGe (Fig. S2 in ESI.†). These calculation results are shown in Fig. 2. In $Si_{57}Ge_6Au_1$, electronic levels coming from Au are formed in bandgap, as shown by the arrow in Fig. 2(d), indicating that isolated substitutional Au impurities, namely point defects, form energy levels near valence band maximum and work as acceptors. On the other hand, in $Si_{56}Ge_6Au_2$ where two substitutional Au impurities are neighboured as indicated by the arrows in Fig. 2(e),

This journal is © The Royal Society of Chemistry 20xx

Please do not adjust margins

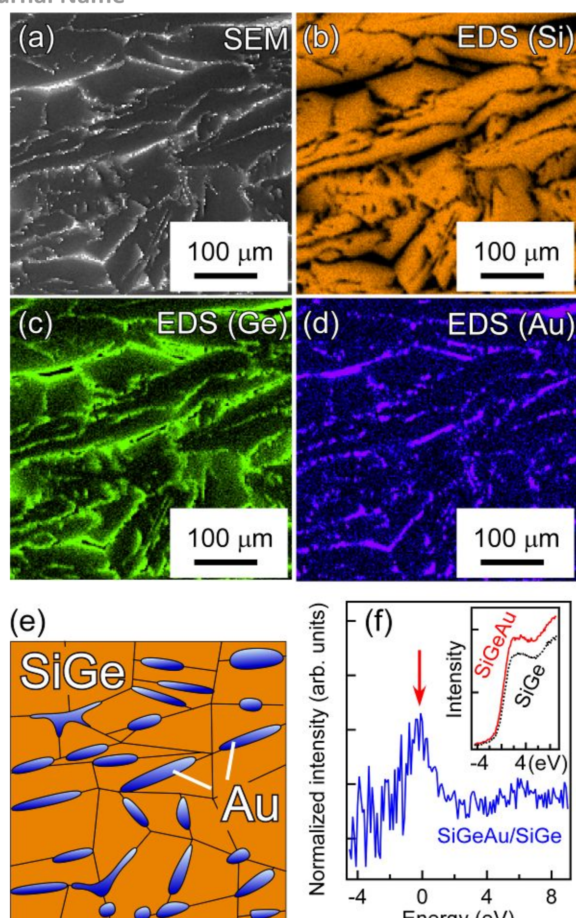

Fig. 3 SEM-EDS images of P-doped SiGeAu sample (P: 1.0 at%): SEM image (a) and elemental maps of Si (b), Ge (c), and Au (d). P was not detectable because of its small amount. (e) Schematic illustration of P-doped SiGeAu sample. (f) Normalized NEXAFS spectrum (SiGeAu/SiGe): NEXAFS spectrum from Ge 2p of undoped SiGeAu divided by that of undoped SiGe. The inset in (f) shows NEXAFS spectra from Ge 2p of undoped SiGeAu (the solid line) and undoped SiGe (the dotted line). Horizontal axis of the inset in (f) is energy relative to Fermi energy (EF).

resonant energy levels appeared in the conduction band (the arrow in Fig. 2(f)). Two substitutional Au impurities form resonant level near conduction band minimum (CBM). We considered that adjacence of two Au atoms is not absolutely necessary for forming resonant level, and resonant level is formed only if the hybridization of two Au atoms and SiGe occurs. Namely, two Au atoms which are separate to some extent can interact with each other through the hybridization with spreading SiGe states, leading to the formation of resonant level. This interaction is similar to Mn-Mn interaction in magnetic semiconductor (Ga, Mn)As with dilute Mn impurities[42]. To confirm this dilute Au impurity effect, we calculated DOS of the separate substitutional Au atoms, indicating that they can form resonant energy level near CBM, as shown in Fig. S3 ESI.†. These results indicate that the dilute substitutional Au impurities is a key for increasing S by RLE. It is also considered that dilute Au impurities, which are more stable than nearest neighbor Au pairs, are possibly formed. Therefore, n-type SiGeAu would be expected for high thermoelectric performance by RLE.

Formation of SiGeAu nanocomposite and its electronic structure.

We fabricated P-doped SiGeAu nanocomposites by suction casting method. The distribution of each constituent element in SiGeAu samples was observed by scanning electron microscopy (SEM) – energy dispersive X-ray spectrometry (EDS). Fig. 3 (a)-(d) show SEM-EDS images: SEM image and elemental maps of Si, Ge, and Au for P-doped SiGeAu sample (P: 1.0 at.%), respectively. It was found that Au was inhomogeneously distributed; Au was mainly aggregated at grain boundaries of SiGe parts, which can work as conductive path. Au was also observed inside SiGe parts. In the SiGe parts, there is inhomogeneous distribution of Ge concentration. SiGe nanograins were also observed by high resolution transmission electron microscope (Fig. S4, ESI.†). The conceptual illustration of this unique structure is shown in Fig. 3(e). From the above inhomogeneous distribution of Au, it is possible that dilute Au impurities exist in SiGe, which can form resonant level near CBM.

We investigated the electronic structures of undoped SiGeAu and SiGe samples by near edge X-ray absorption fine structure (NEXAFS) of transition from Ge 2p at RT. The inset in Fig. 3(f) shows each NEXAFS spectrum of undoped SiGeAu and SiGe. Undoped SiGeAu spectrum was divided by undoped SiGe spectrum to obtain normalized NEXAFS spectrum (SiGeAu/SiGe), as shown in Fig. 3(f). In Fig. 3(f), a peak was observed near 0 eV. The results experimentally demonstrated that there are resonant levels near CBM in SiGeAu, which supports the above electronic structure calculation of SiGe with substitutional Au atoms. We succeeded in the formation of resonant levels in SiGe, which can be related to dilute Au impurities, indicating that RLE-$S^2\sigma$ enhancement can be expected in the n-type SiGeAu samples.

Thermoelectric properties.

We measured thermoelectric properties (σ and S) of P-doped SiGeAu and SiGe samples at RT. Fig. 4(a) and (b) show σ and S as a function of the P amount. We confirmed that σ values of both SiGeAu (solid circles) and SiGe samples (solid squares) increased as the P amount increased, which is usual tendency of doping. We found that σ of SiGeAu samples were much higher than that of SiGe samples. This higher σ came from high carrier conductivity of Au. In Fig. 4(b), the S values of both P-doped SiGeAu and SiGe samples were negative, indicating n-type conduction. Fig. 4(c) and (d) show S and $S^2\sigma$ as a function of σ with the data of other SiGe-based materials[5,43-50]. SiGeAu sample (solid circles) exhibited higher S at σ of around 1000 $\Omega^{-1}cm^{-1}$ than other SiGe-based materials. On the other hand, at σ of < ~600 $\Omega^{-1}cm^{-1}$, SiGeAu sample (solid circles) exhibited lower S than SiGe sample (solid squares). It should be noted that a peak of S was observed around 1000 $\Omega^{-1}cm^{-1}$ (solid circles). As a result, SiGeAu sample exhibited about twice higher $S^2\sigma$ at RT than that of SiGe sample and the highest $S^2\sigma$ among the other SiGe-based materials that have ever been reported[5,43-50], as shown in Fig. 4(d).

Here, we discuss the following two points in Fig. 4(c): (1) SiGeAu sample exhibited lower S than that of SiGe sample at σ of < ~600 $\Omega^{-1}cm^{-1}$ and (2) the S tendency like a peak was emergent at ~1000 Ω^{-}

Please do not adjust margins

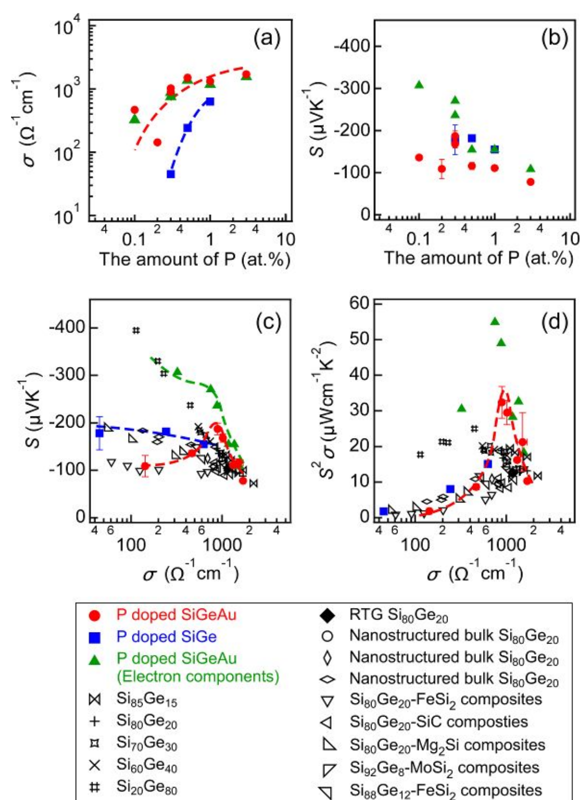

Fig. 4 Thermoelectric properties of SiGeAu (the solid circles) and SiGe (the solid squares) samples at RT. The P amount dependence of the σ (a) and the S values (b). The σ dependence of S (c) and $S^2\sigma$ values (d) with the values of other SiGe-related materials. Electron contributions of P-doped SiGeAu (S_e, σ_e, and $S_e^2\sigma_e^2$) are shown by the solid triangles. Dashed lines in (a), (c) and (d) are eye guides.

^{1}cm^{-1}. We confirmed that these do not come from the difference of mass density due to the similar mass density in each sample (Table S1 and S2, ESI.†). It is possible that the lower S of SiGeAu sample at σ of < ~600 Ω^{-1}cm^{-1} comes from bipolar conduction: conduction of electrons and holes generated by P dopants and defect-related acceptors (isolated Au impurities), respectively. As shown by the calculation result in Fig. 2(b), isolated Au impurities might work as an acceptor. Actually, when P dopant amount was very low in SiGeAu sample (<0.05 at.%), p-type conduction was observed (not shown). It should be noted that Hall carrier concentration of ~2×10^{20} cm^{-3} (hole concentration) in such p-type SiGeAu sample with low P amount was larger than that of undoped p-type SiGeAu sample (2×10^{19} cm^{-3} (hole concentration)) even though P dopants in SiGe work as donors. This result denies complete carrier compensation between P donor and defect-related acceptor, revealing bipolar conduction. This detail is shown in the ESI.†. This bipolar conduction seems to come from the inhomogeneous distribution of Au concentration (isolated Au impurities and dilute Au impurities) due to the fabrication method of suction casting method, as shown in Fig. 3(d).

To extract the essential properties of P-doped SiGeAu samples without defects causing bipolar conduction, we considered transport properties by using the following equations:

$$\sigma_{meas} = \sigma_e + \sigma_h \qquad (1)$$

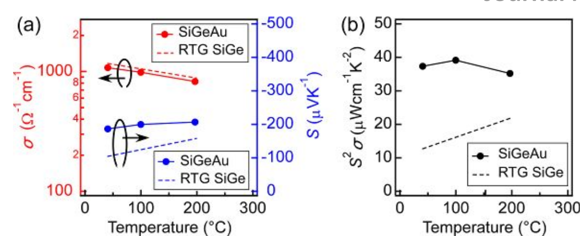

Fig. 5 The temperature dependence of the σ (left axis) and the S (right axis) (a), and the $S^2\sigma$ (b) of P-doped SiGeAu (0.3 at.% P atoms) and RTG SiGe.

$$S_{meas} = \frac{S_e\sigma_e + S_h\sigma_h}{\sigma_{meas}} \qquad (2),$$

where the indices "meas", "e", and "h" describe measured value of the samples, and electron and hole contributions, respectively. The electron contributions to S and σ of SiGeAu sample (S_e and σ_e) are shown by the triangle marks in Fig. 4 (a)-(c). The electron contributions are the essential properties of P-doped (n-type) SiGeAu samples without defects generating holes. In Fig. 4(a) and (b), σ_e of SiGeAu sample was much higher than σ of SiGe sample, and S_e of SiGeAu sample was higher than S of SiGe sample. This simultaneous enhancement of σ and S has not been found in other reports of $S^2\sigma$ enhancement by RLE. This simultaneous enhancement implies a success of $S^2\sigma$ enhancement by "thermal management" with RLE, bringing the possibility of about four times $S^2\sigma$ enhancement to ~ 55 μWcm^{-1}K^{-2} (the triangles in Fig. 4(d)) at RT, which exceeds that of Bi_2Te_3. In Fig. 4(c), there seems to be a hump of S_e (solid triangles) indicated by the dashed curve, which is the same as a peak position of S of SiGeAu samples (solid circles). We also observed the unique tendency from carrier concentration dependence of S (Fig. S5 ESI.†). This unique tendency, which is consistent with that of materials having resonant level[37], demonstrates $S^2\sigma$ enhancement by RLE. From these results, this high $S^2\sigma$ of SiGeAu sample was found to come from three factors: (1) Au crystals increased σ as conductive path. (2) Au impurities brought RLE and phonons scattering, resulting in enhanced S and lowered κ of SiGe parts. (3) This enhanced high S is available as the effective S of the entire nanocomposites because temperature difference is applied to SiGe parts with lowered κ, not to Au crystals with low S. This thermal management with RLE succeeded in compensating the weakness (σ degradation) of RLE approach, realizing further $S^2\sigma$ enhancement: simultaneous increase of σ and S. On the other hand, bipolar conduction coming from defects reduce S, leading to $S^2\sigma$ reduction. However, this problem would be solved by removing such defects. This methodology of $S^2\sigma$ enhancement is a universal method with applicability to other thermoelectric materials.

We measured σ, S and $S^2\sigma$ of SiGeAu sample (P: 0.3 at.%) at RT-200 ˚C, as shown in Fig. 5. Therein, the data of radioisotope thermoelectric generator (RTG) SiGe are also plotted for reference[5]. SiGeAu sample and RTG SiGe showed similar tendency of both σ and S. S of SiGeAu sample was higher than that of RTG SiGe while both σ values were almost the same. As a result, SiGeAu sample exhibited 2-3 times higher $S^2\sigma$ than RTG SiGe at RT-200 ˚C, as shown in Fig. 5(b). The κ values of SiGeAu (P: 0.3 at.%, P: 1.0 at.%) samples were

This journal is © The Royal Society of Chemistry 20xx
Please do not adjust margins

Table 1 σ, κ, κ_{lat}, and ZT at RT of P-doped SiGeAu sample with those of RTG SiGe[5].

Sample	σ [Ω^{-1}cm^{-1}]	κ [Wm^{-1}K^{-1}]	κ_{lat} [Wm^{-1}K^{-1}]	ZT @ RT
SiGeAu (P: 0.3 at.%)	0.9×10^3	6.7	5.6	0.15
SiGeAu (P: 1.0 at.%)	1.3×10^3	4.8	3.8	0.10
RTG SiGe (P: 2.0 at.%)	1.2×10^3	4.6	3.7	0.08

measured at RT. Table 1 shows κ values of SiGeAu (P: 0.3 at.%, P: 1.0 at.%) samples and RTG SiGe[5]. Therein, lattice thermal conductivity κ_{lat} and ZT values are also shown. κ_{lat} is calculated from Wiedemann-Frantz law by using the following equation:

$$\kappa_{lat} = \kappa - L\sigma T \quad (3)$$

where L is Lorentz number (~2.4×10^{-8} WΩK^{-2}). κ of SiGeAu sample was almost the same value as that of RTG SiGe at the same σ. Table 1 shows that κ of SiGeAu samples decreased as P amount increased. This reduction by P doping indicates that P dopants in SiGe parts also work as phonon scattering centers. Finally, we calculated ZT values of SiGeAu samples at RT, which is shown in Table 1. SiGeAu sample (P: 0.3 at.%) exhibited about twice higher ZT than that of RTG SiGe due to high $S^2\sigma$. This high ZT value was obtained by thermal management with RLE.

Conclusion

We present the methodology for $S^2\sigma$ enhancement: thermal management with RLE for simultaneous enhancement of σ and S of SiGe, unlike other reports of $S^2\sigma$ enhancement by RLE. In P-doped SiGeAu sample fabricated by suction casting method, Au was distributed at grain boundary, which is suitable to thermal control. The calculation of electronic states and NEXAFS measurement support the existence of resonant level, which enhances S. SiGeAu samples exhibited the highest $S^2\sigma$ at RT among SiGe-related materials that have ever been reported. κ of SiGeAu sample was comparable to RTG SiGe. As a result, SiGeAu sample exhibited much higher ZT than that of RTG SiGe at RT. This methodology: thermal management with RLE related to the simultaneous control of electronic states and heat flow provides a guideline for enhancement of thermoelectric performance.

Experimental section

Material synthesis

SiGeAu ($Si_{79}Ge_{19}Au_2$) and SiGe ($Si_{80}Ge_{20}$) samples were fabricated by suction casting method[38,51]. Alloy ingots of Si (5N), Ge (5N), Au (4N), and P (7N) (donor impurity) were arc melted for $Si_{79}Ge_{19}Au_2$ while alloy ingots for $Si_{80}Ge_{20}$ were composed of Si (5N), Ge (5N), and P (7N). Then, melted materials were quenched in a cylinder by suctioning through evacuation system to form bulk alloy ingots. The suctioning speed is 1000 mms^{-1}. Obtained bulk alloy ingots have diameters of 5 mm and lengths of around 30 mm, which were cut into 8 mm-thick pieces for measurements of S and σ, and 2 mm-thick disks for κ measurement.

Calculation of electronic structures

Electronic structures of SiGe and SiGeAu based on DFT first-principle calculation with Wien2k software package. Therein, we use the k-points grid sampling of 5×5×5 for $Si_{56}Ge_6$, 14×14×14 for $Si_{57}Ge_6Au_1$ and $Si_{56}Ge_6Au_2$.

Characterization

Distributions of the constituent elements were measured by SEM-EDS. The electronic structures were measured by NEXAFS. The S and σ were measured by ZEM-3 (Advance Riko, Inc.) and the κ was measured by laser flash method, in the longitudinal direction of cylinder. For confirmation, κ was also measured by 2ω method[52]. Characterizations were mainly done at RT.

Conflicts of interest

There are no conflicts to declare.

Acknowledgements

This work was supported in part by JST CREST Grant No. JPMJCR1524, and Grant-in-Aid for Scientific Research A (Grant No. 19H00853) and for Exploratory Research (No. 19K22110) from JSPS KAKENHI, Japan. The authors would like to thank Dr. S. Ikeuchi from ADVANCE RIKO Inc. for the thermal conductivity measurement by laser flash method.

References

1 S. K. Bux, R. G. Blair, P. K. Gogna, H. Lee, G. Chen, M. S. Dresselhaus, R. B. Kaner, J. P. Fleurial, *Adv. Func. Mater.* 2009, **19**, 2445-2452.
2 A. I. Hochbaum, R. Chen, R. D. Delgado, W. Liang, E. C. Garnett, M. Najarian, A. Majumdar, P. Yang, *Nature* 2008, **451**, 163-167.
3 A. I. Boukai, Y. Bunimovich, J. T. Kheli, J. K. Yu, W. A. Goddard, J. R. Heath, *Nature* 2008, **451**, 168-171.
4 G. Joshi, H. Lee, Y. Lan, X. Wang, G. Zhu, D. Wang, R. W. Gould, D. C. Cuff, M. Y. Tang, M. S. Dresselhaus, G. Chen, Z. Ren, *Nano Lett.* 2008, **8**, 4670-4674.
5 X. W. Wang, H. Lee, Y. C. Lan, G. H. Zhu, G. Joshi, D. Z. Wang, J. Yang, A. J. Muto, M. Y. Tang, J. Klatsky, S. Song, M. S. Dresselhaus, G. Chen, Z. F. Ren, *Appl. Phys. Lett.* 2008, **93**, 193121.
6 K. Biswas, J. He, I. D. Blum, C. I. Wu, T. P. Hogan, D. N. Seidman, V. P. Dravid, M. G. Kanatzidis, *Nature* 2012, **489**, 414-418.
7 Y. Nakamura, M. Isogawa, T. Ueda, S. Yamasaka, H. Matsui, J. Kikkawa, S. Ikeuchi, T. Oyake, T. Hori, J. Shiomi, A. Sakai, *Nano Energy* 2015, **12**, 845-851.
8 S. Yamasaka, Y. Nakamura, T. Ueda, S. Takeuchi, A. Sakai, *Sci. Rep.* 2015, **5**, 14490.
9 Y. Nakamura, *Sci. Technol. Adv. Mater.* 2018, **19**, 31-43.
10 T. Oyake, L. Feng, T. Shiga, M. Isogawa, Y. Nakamura, J. Shiomi, *Phys. Rev. Lett.* 2018, **120**, 045901.
11 A. Samarelli, L. F. Llin, S. Cecchi, J. Frigerio, T. Etzelstorfer, E. Müller, Y. Zhang, J. R. Watling, D. Chrastina, G. Isella, J. Stangl,

This journal is © The Royal Society of Chemistry 20xx

Please do not adjust margins

J. P. Hague, J. M. R. Weaver, P. Dobson, and D. J. Paul, *J. Appl. Phys.* 2013, **113**, 233704.
12 L. F. Llin, A. Samarelli, S. Cecchi, T. Etzelstorfer, E. M. Gubler, D. Chrastina, G. Isella, J. Stangl, J. M. R. Weaver, P. S. Dobson, and D. J. Paul, *Appl. Phys. Lett.* 2013, **103**, 143507.
13 S. Kong, T. Wu, M. Yuan, Z. Huang, Q. L. Meng, Q. Jiang, W. Zhuang, P. Jiang, and X. Bao, *J. Mater. Chem. A* 2017, **5**, 2004.
14 G. Schierning, *Phys. Status Solidi A* 2014, **211**, 1235-1249.
15 K. Biswas, J. He, Q. Zhang, G. Wang, C. Uher, V. P. Dravid, M. G. Kanatzidis, *Nat. Chem.* 2011, **3**, 160-166.
16 S. Yamasaka, K. Watanabe, S. Sakane, S. Takeuchi, A. Sakai, K. Sawano, and Y. Nakamura, *Sci. Rep.* 2016, **6**, 22838.
17 H. Ohta, S. Kim, Y. Mune, T. Mizoguchi, K. Nomura, S. Ohta, T. Nomura, Y. Nakanishi, Y. Ikuhara, M. Hirano, H. Hosono, K. and Koumoto, *Nat. Mater.* 2008, **6**, 129-134.
18 A. M. Dehkordi, M. Zebarjadi, J. He, T. M. Tritt, *Mater. Sci. Eng. R* 2015, **97**, 1-22.
19 Pei, Y., Shi, X., LaLonde, A., Wang, H., Chen, L., Snyder, G. J. Convergence of Electronic Bands for High Performance Bulk Thermoelectrics. Nature 473, 66-69 (2011).
20 Y. Tang, Z. M. Gibbs, L. A. Agapito, G. Li, H. S. Kim, M. B. Nardelli, S. Curtarolo, G. J. Snyder, *Nat. Mater.* 2015, **14**, 1223-1228.
21 J. P. Heremans, V. Jovovic, E. S. Toberer, A. Saramat, K. Kurosaki, A. Charoenphakdee, S. Yamanaka, G. J. Snyder, *Science* 2008, **321**, 554-557.
22 J. Zhang, R. Liu, N. Cheng, Y. Zhang, J. Yang, C. Uher, X. Shi, L. Chen, W. Zhang, *Adv. Mater.* 2014, **26**, 3848-3853.
23 D. Vashaee, A. Shakouri, *Phys. Rev. Lett.* 2014, **92**, 106103.
24 X. Zianni, D. Narducci, *Nanoscale* 2019, **11**, 7667-7673.
25 T. Ishibe, A. Tomeda, K. Watanabe, Y. Kamakura, N. Mori, N. Naruse, Y. Mera, Y. Yamashita, Y. Nakamura, *ACS Appl. Mater. Interfaces* 2018, **10**, 37709-37716.
26 S. Sakane, T. Ishibe, T. Taniguchi, N. Naruse, Y. Mera, T. Fujita, M. M. Alam, K. Sawano, N. Mori, and Y. Nakamura, *Mater. Today Energy* 2019, **13**, 56-63.
27 T. Taniguchi, T. Ishibe, N. Naruse, Y. Mera, M. M. Alam, K. Sawano, and Y. Nakamura, *ACS Appl. Mater. Interfaces* 2020, **12**, 25428-25434.
28 J. P. Hereman, B. Eiendlocha, and A. M. Chamoire, *Energy Environ. Sci.* 2012, **5**, 5510-5530.
29 J. P. Heremans, V. Jovovic, E. S. Toberer, A. Saramat, K. Kurosaki, A. Charoenphakdee, S. Yamanaka, and G. J. Snyder, *Science* 2008, **321**, 554-557.
30 N. Narendra, P. Norouzzadeh, D. Vashaee, and K. W. Kim, *Appl. Phys. Lett.* 2017, **111**, 232101.
31 F. Guo, B. Cui, H. Geng, Y. Zhang, H. Wu, Q. Zhang, B. Yu, S. J. Pennycook, W. Cai, and J. Sui, *Small* 2019, **15**, 1902493.
32 M. Li, Y. Luo, G. Cai, X. Li, X. Li, Z. Han, X. Lin, D. Sarker, and J. Cui, *J. Mater. Chem. A* 2019, **7**, 2360-2367.
33 M. Zebarjadi, K. Esfarjani, M. S. Dresselhaus, Z. F. Ren, and G. Chen, *Energy Environ. Sci.* 2012, **5**, 5147-5162.
34 W. Lu, T. He, S. Li, X. Zuo, Y. Zheng, X. Lou, J. Zhang, D. Li, J. Liu, and G. Tang, *Nanoscale* 2020, **12**, 5857-5865.
35 P. Hu, T. R. Wei, P. Qiu, Y. Cao, J. Yang, X. Shi, and L. Chen, *ACS Appl. Mater. Interfaces* 2019, **11**, 34046-34052.
36 H. Tan, L. Guo, G. Wang, H. Wu, X. Shen, B. Zhang, X. Lu, G. Wang, X. Zhang, and X. Zhou, *ACS Appl. Mater. Interfaces* 2019, **11**, 23337-23345.
37 Z. Pan, and H. Wang, *J. Mater. Chem. A* 2019, **7**, 12859-12868.
38 S. Sakane, T. Ishibe, K. Mizuta, M. Kashino, K. Watanabe, T. Fujita, Y. Kamakura, N. Mori, and Y. Nakamura, *ACS Appl. Energy Mater.* 2020, **3**, 1235-1241.
39 S. M. Sze, and J. C. Irvin, *Solid State Electron.* 1968, **11**, 599.
40 K. Fukushima, and N. Kondo, *Jpn. J. Appl. Phys.* 2001, **40**, 3226-3230.
41 P. Blaha, K. Schwarz, G. Madsen, D. Kvasnicka, and J. Luitz, *WIEN2K, an augmented plane wave plus local orbitals program for calculating crystal properties.* Vienna University of Technology, Austria, 2001.
42 J. Ohe, Y. Tomoda, N. Bulut, R. Arita, K. Nakamura, S. Maekawa, J. Phys. Soc. Jpn. 2009, **78**, 083703.
43 J. P. Dismukes, L. Ekstrom, E. F. Steigmeier, I. Kudman, and D. S. Beers, *J. Appl. Phys.* 1964, **35**, 2899-2907.
44 A. A. Usenko, D. O. Moskovskikh, M. V. Gorshenkov, A. V. Korotitskiy, S. D. Kaloshkin, A. I. Voronin, and V. V. Khovaylo, *Scripta Mater.* 2015, **96**, 9-12.
45 R. Murugasami, P. Vivekanandhan, S. Kumaran, R. S. Kumar, and T. J. Tharakan, *Scripta Mater.* 2018, **143**, 35-39.
46 A. Usenko, D. Moskovskikh, A. Korotitskiy, M. Gorshenkov, A. Voronin, D. Arkhipov, M. Lyange, G. Isachenko, and V. Khovaylo, *J. Electron. Mater.* 2016, **45**, 3427-3432.
47 S. Bathula, M. Jayasimhadri, B. Gahtori, A. Kumar, A. K. Srivastava, and A. Dhar, *Phys. Chem. Chem. Phys.* 2017, **19**, 25180-25185.
48 A. Usenko, D. Moskovskikh, A. Korotitskiy, M. Gorshenkov, E. Zakharova, A. Fedorov, Y. Parkhomenko, V. Khovaylo, *Scripta Mater.* 2018, **146**, 295-299.
49 K. Favier, G. B. Granger, C. Navone, M. Soulier, M. Boidot, J. Leforestier, J. Simon, J. C. Tedenac, and D. Ravot, *Acta Mater.* 2014, **64**, 429-442.
50 A. Nozariasbmarz, Z. Zamanipour, P. Norouzzadeh, J. S. Krasinski, and D. Vashaee, *RSC Adv.* 2016, **6**, 49643-49650.
51 A. Inoue, T. Zhang, *Mater. Trans., JIM* 1995, **36**, 1184.
52 K. Mitarai, R. Okuhata, J. Chikada, T. Kaneko, Y. Uematsu, Y. Komatsubara, T. Ishibe, Y. Nakamura, *J. Appl. Phys.* 2020, **128**, 015102.

This journal is © The Royal Society of Chemistry 20xx

Please do not adjust margins